Current Nanoscience, 2021, *17*, 646-657

RESEARCH ARTICLE

Iron Oxide Nanoparticles Synthesized *Via* Green Tea Extract for Doxorubicin Delivery

Lei Nie[1,2,#,*], Chenlei Cai[3,#], Meng Sun[1], Fang Zhang[4], Lingyun Zheng[5], Qi Peng[6], Amin Shavandi[7,*] and Shoufeng Yang[2]

[1]*Henan Key Laboratory of Tea Plant Biology, College of Life Sciences, Xinyang Normal University, Xinyang 464000, China;* [2]*Department of Mechanical Engineering, Member of Flanders Make, KU Leuven (Catholic University of Leuven), Leuven 3001, Belgium;* [3]*Department of Traditional Chinese Medicine, Hebei General Hospital, Shijiazhuang 050000, China;* [4]*College of Life Science & Technology, Huazhong University of Science and Technology, Wuhan 430074, China;* [5]*Analysis & Testing Center, Xinyang Normal University, Xinyang 464000, China;* [6]*College of Chemistry and Chemical Engineering, Xinyang Normal University, Xinyang, Henan 464000, China;* [7]*BioMatter-Biomass Transformation Lab (BTL), Université Libre de Bruxelles, Avenue F.D. Roosevelt, 50 - CP 165/61, 1050 Brussels, Belgium*

Abstract: ***Background*:** Due to the limitation of conventional cancer treatment using chemotherapy, the nanoparticle therapeutics have shown enhanced efficacy with alleviating side effects.

***Objective*:** The aim of this study was to prepare the superparamagnetic iron oxide nanoparticles (T-C-SPION) for doxorubicin (DOX) loading and delivery.

***Methods*:** Here, we reported a simple green strategy to fabricate T-C-SPION using green tea extract and citric acid. Also, the anti-cancer drug, DOX, was used as a model drug to fabricate DOX-loaded nanoparticles.

***Results*:** The formed T-C-SPION nanoparticles were spherical with a diameter of 23.8 ± 0.8 nm, as confirmed by Transmission Electron Microscopy (TEM). Besides, Dynamic Light Scattering (DLS) revealed that the prepared nanoparticles were water-dispersible and stable while stored in water for 6 weeks. The CCK-8 assay showed T-C-SPION to have a good cytocompatibility using different iron concentrations (10 ~ 120 ug/mL). Furthermore, T-C-SPION had a higher DOX encapsulation efficiency (E_{encaps}), around 43.2 ± 1.8 %, which resulted in a lagged release profile of DOX, compared to other types of iron oxide nanoparticles using green tea or citric acid alone. Next, cell viability assay indicated that T-C-SPION with a higher E_{encaps} showed superior and sustained cytotoxicity compared to the control group.

***Conclusion*:** The developed iron oxide nanoparticles synthesized by green tea extract and citric acid in this paper could be considered as a potential drug carrier for cancer therapy applications.

Keywords: Nanoparticles, iron oxide, green tea, citric acid, doxorubicin, drug delivery, cytocompatibility.

ARTICLE HISTORY

Received: February 21, 2020
Revised: August 31, 2020
Accepted: September 18, 2020

DOI:
10.2174/1573413716999201029205654

1. INTRODUCTION

Since Shen Nung, the second Chinese emperor, discovered tea from the plant *Camellia sinensis* in 2700 BC; this beverage has become one of the most popular drinks in the world since thousands of years. Due to the high levels of antioxidant polyphenols in tea, the consumption of tea could result in reducing the risk of cancer, and lowering blood pressure, and so on [1-4]. Compared to black tea and oolong tea, green tea, "non-fermented" tea, contains more catechins, which have active antioxidant activities both *in vitro* and *in vivo*. Furthermore, the vitamins and minerals (vary in different concentrations from different places) in green tea increase the antioxidant potential [5]. Green tea has been considered a healthy beverage by traditional Chinese medicine [6]. Epidemiological data showed that green tea, instead of "fermented" tea, could prevent breast and prostate cancers, mainly due to the inhibition of urokinase by epigallocatechin-3 gallate (EGCG) in green tea. Also, green tea could

*Address correspondence to these authors at the Henan Key Laboratory of Tea Plant Biology, College of Life Sciences, Xinyang Normal University (XYNU), Xinyang 464000, China; Tel: +32 485656079;
E-mail: nieleifu@yahoo.com; nielei@xynu.edu.cn;
BioMatter-Biomass Transformation Lab (BTL), Université Libre de Bruxelles, Avenue F.D. Roosevelt, 50 - CP 165/61, 1050 Brussels, Belgium; Tel: +32 (0) 26503681; E-mail: amin.shavandi@ulb.ac.be
[#]*These authors contributed equally to this work.*

enhance immune function [7]. On the other hand, green tea could be applied in the preparation of nanoparticles as a drug delivery system for cancer therapy [8].

Conventional cancer treatment using chemotherapy has limitations such as nonselective distribution of drugs, insufficient therapeutic efficacy, and unsustainable drug release. National Cancer Data Base shows that the number of cancer survivors increases year by year because of advances in early detection and treatments [9]. Nowadays, cancer treatment has evolved from relatively non-specific cytotoxic agents to selective therapeutics [10], such as oncolytic virus therapy [11], nanoparticles-mediated thermal therapies [12], nanocages-photothermal transducers [13], *etc*. The clinical data confirmed that nanoparticle therapeutics showed enhanced efficacy, and due to the favorable anti-cancer drug pharmacokinetics and tunable biodistribution of nanoparticles, the side effects were alleviated [14-16]. Iron supplement ferumoxytol and other iron oxide nanoparticles were approved by the Food and Drug Administration (FDA) for magnetic resonance imaging and drug carriers [17]. Superparamagnetic iron oxide nanoparticles (SPION) have attracted significant interest in biomedical applications due to their superparamagnetic properties, biocompatibility, and biodegradability. The modified SPION can be applied for separation (*e.g*., cell sorting), therapy (*e.g*., hyperthermia), and diagnosis (*e.g*., cell tracking) [18]. SPION shows advantages for cancer treatment, such as by generating local heat when exposed to an alternating magnetic field [17, 19]. Also, SPION can be rapidly taken up by the reticuloendothelial system (RES) to detect tumor lesions in the liver. Due to the smaller size of SPION (less than 50 nm), it can escape phagocytosis with a prolonged circulation time to reach inflammation sites or tumors [20, 21]. In this paper, the potential of magnetic iron oxide nanoparticles for diagnosis as well as therapy for cancer via the release of anti-cancer drugs has been shown.

The SPION can be prepared by a chemical precipitation method [22-29]. However, the SPION tends to aggregate due to the nanoscale size and abundant surface energy of SPION, and such aggregation further decreases the stability of the colloidal nanoparticle dispersion [30]. In 2004, a high-temperature synthesis method was first reported by Park *et al.* to prepare ultra-large-scaled monodisperse iron oxide nanoparticles using iron oleate composite as a precursor [31]. Monodisperse SPION with a tunable range of size (around 2-30 nm) could be synthesized by organic thermal decomposition using different iron-containing precursors, such as iron pentacarbonyl and iron oxyhydroxide [32]. Whereas the hydrophobic dispersant shell on the surface of SPION influences its stability in cell medium and further limits its biomedical applications. Hydrophilic molecular links could replace the hydrophobic molecules on the surface of SPION via the ligand exchange method [33, 34]. Many biocompatible polymers, such as poly(ethylene glycol) (PEG) [35], polyethyleneimine (PEI) [36], and poly(vinyl alcohol) (PVA) [18], polysaccharide [37], *etc.*, have been successfully used as capping and stabilizing agents on the surface of SPION [23, 38-40]. Nonetheless, the unstable ligand shell may lead to strong agglomeration of the SPION (large clusters formed) and, therefore, increases the inhomogeneity. Such inhomogeneous property of SPION would decrease the loading efficiency of drugs and their sustained release, especially under physiological conditions.

Recently, flavonoids, particularly catechins, which are of great abundance in green tea, have received a large amount of attention due to the strong binding formed between SPION and bioactive macromolecules via hydrogen binding and π-π stacking interaction [41]. The green tea leaf extracts containing polyphenols act as a reducing agent and a capping agent for the synthesis of SPION [42, 43]. Nune *et al*. confirmed that the tea phytochemicals such as catechins and theaflavins served a dual role as reducing agents and stabilizers during the nanoparticle formation [1]. However, the diameter of SPION was difficult to regulate using the above methods. There are few reports on monodisperse SPION fabricated by green tea leaf extract [44-46].

Here we report a simple green strategy to fabricate SPION *via* green tea (Scheme **1**). The morphology, size distribution, stability, and cytocompatibility of prepared SPION were evaluated by Transmission Electron Microscopy (TEM), Dynamic Light Scattering (DLS), zeta potentials, and CCK-8 analysis. Also, the anti-cancer drug, doxorubicin (DOX), was used as a model drug to fabricate DOX-loaded SPION; then the encapsulation efficiency (E_{encaps}) and release profiles of DOX were systematically investigated. The obtained *in vitro* data suggested that DOX-loaded SPION is promising for cancer therapy.

2. MATERIALS AND METHODS

2.1. Materials

Iron (III) chloride hexahydrate ($FeCl_3 \cdot 6H_2O$), Iron (II) chloride tetrahydrate ($FeCl_2 \cdot 4H_2O$), ammonia solution (25%, NH_4OH), and citric acid were purchased from Sigma-Aldrich Co., Ltd. DOX·HCl was obtained from URchem Co., Ltd. Green tea (Brand: Xinyang Maojian Tea, as the Top 10 teas in China, picked from Xinyang city, China) was provided by Henan Key Laboratory of Tea Plant Biology. All other chemicals were purchased from China National Medicines Corporation Ltd. (analytical grade).

2.2. Preparation of Green Tea Leaf Extract Solution

The green tea leaves were first washed by Millipore water at least 3 times. When the temperature of the water was increased to 100°C, the green leaves were added and kept for 30 min; note that the green tea/water ratio was 0.02 g/mL. Then, the mixture solution was considered as the green tea leaf extract solution for the following iron oxide nanoparticle preparation.

2.3. Synthesis of Iron Oxide Nanoparticles *Via* Citrate and Green Tea (T-C-SPION)

7.39 g $FeCl_3 \cdot 6H_2O$ (4.44 g of $FeCl_3$) and 2.714 g $FeCl_2 \cdot 4H_2O$ (1.732 g of $FeCl_2$) were dissolved in 80 mL of prepared green tea leaf extract solution in a flask and stirred at 70°C in refluxing condition under nitrogen atmosphere for 30 min; then 20 mL of ammonia solution was added slowly and kept at the same temperature for another 30 min. Afterward, 2g of citric acid was dissolved in water and was added to the above reaction solution; the temperature was de-

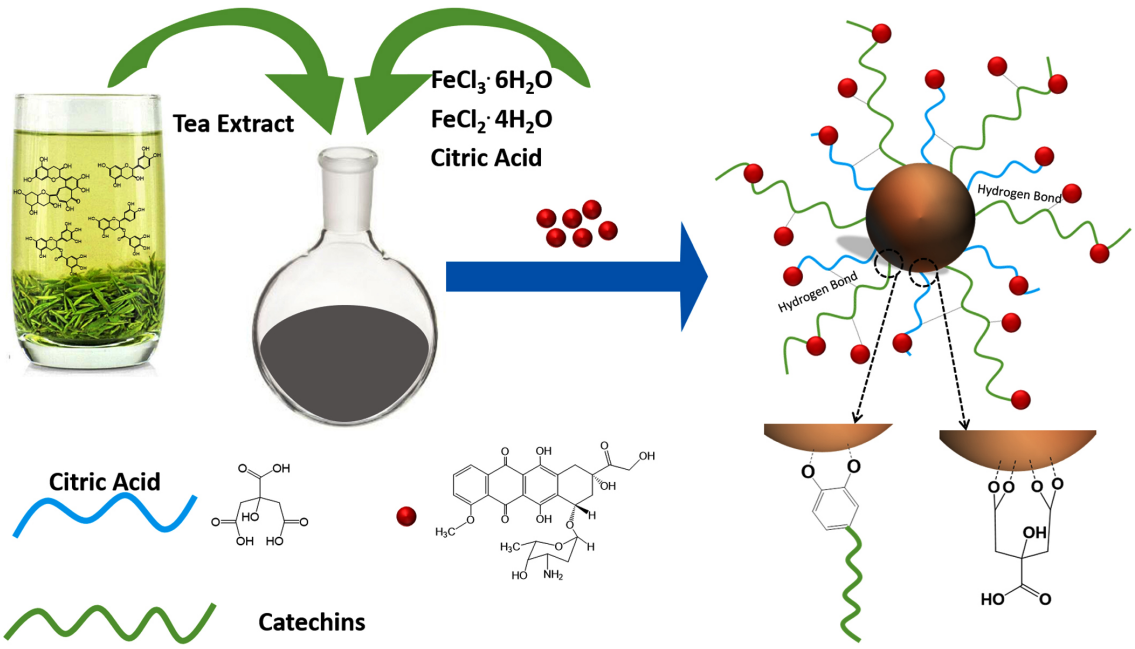

Scheme 1. Schematic illustration for the preparation of superparamagnetic iron oxide nanoparticles (SPION) via green tea extract and citric acid for the doxorubicin delivery system; the hydrogen bonds exist between citric acid, catechins, and doxorubicin. (*A higher resolution / colour version of this figure is available in the electronic copy of the article*).

creased to room temperature (RT) and the solution was stirred for 24 h. Finally, a permanent magnet was used to obtain the black colored precipitates, which were thoroughly rinsed with Millipore water, to get T-C-SPION nanoparticle. At the same time, bare SPION without using both green tea extract and citric acid, and SPION with using only citric acid (represented as C-SPION), and SPION with using only green tea (represented as T-SPION) were also prepared for comparison (Electronic Supplementary Material).

2.4. Characterization of Prepared Nanoparticles

First, the prepared nanoparticles were examined by X-ray diffraction (XRD, Smartlab9) and Fourier Transform Infrared (FT-IR, PerkinElmer, Spectrum 2). Then, the morphology of nanoparticles was characterized by FEI-Transmission Electron Microscopy (TEM, Tecnai G2 F20), and the diameters of dry nanoparticles were statistically analyzed by Fiji software *via* over 10 TEM images. The hydrodynamic radius of SPION was tested by Dynamic Light Scattering (DLS, Malvern Zetasizer 3000E); during the DLS test, the pH of SPION dispersed water was tested at around 7, and the stability of SPION in solution was also measured by zeta potential. Next, the iron concentration of nanoparticles was measured by Atomic Absorption Spectroscopy (AAS, Thermo Scientific iCETM 3400, Electronic Supplementary Material).

2.5. Preparation of DOX-loaded Nanoparticles

DOX-loaded bare SPION, DOX-loaded T-SPION, DOX-loaded C-SPION, and DOX-loaded T-C-SPION were prepared, respectively. DOX (10 mg) and prepared nanoparticles (0.5 mL, 20 mg/mL) were dispersed in 4.5 mL Millipore water, stirred for 24 h at RT. The nanoparticles were separated by ultracentrifugation for 1 h at 30 000 g and washed with Millipore water 3 times to remove unloaded DOX, and then the nanoparticles were vacuum-dried. The DOX encapsulation efficiency (E_{encaps}) was measured by using a UV-Vis spectrophotometer (Agilent Cary5000). The DOX E_{encaps} is given as (Eq. 1):

$$E_{encaps}\ (\%) = \frac{M_{feed} - M_{residual}}{M_{feed}} \times 100\ \% \qquad (1)$$

Where, the M_{feed} and $M_{residual}$ values are the total feed amount and the DOX amount in the solution after centrifugation, respectively.

2.6. Release Profiles of DOX-loaded Nanoparticles

The release profiles of DOX from DOX-loaded bare SPION, DOX-loaded T-SPION, DOX-loaded C-SPION, and DOX-loaded T-C-SPION were investigated respectively. First, 1 mg of DOX-loaded nanoparticles were injected into a 20 kDa MWCO dialysis cassette (Thermo ScientificTM Slide-A-LyzerTM). Then, the cassette was placed in a release buffer of 80 mL PBS with 5% BSA and stirred at 37°C (pH: 7.35 ~ 7.45). At predetermined time points, 100 µL aliquots were collected and replaced with fresh buffer. The DOX fluorescence intensity of the aliquots was measured using a UV-Vis spectrophotometer (Agilent Cary5000); finally, the cumulative release of DOX was calculated [47].

2.7. Cell Culture

Regarding that, the potential applications of prepared nanoparticles for lung cancer and wearable biomedical devices, A549 lung epithelial cells (ATCC® CCL-185), and HaCat cells (ATCC® HB-241TM) were used. According to ATCC instructions, cells were grown in Dulbecco's modified Eagle's medium (DMEM) (Sigma-Aldrich) supplemented with

10% fetal bovine serum, 100 U mL^{-1} penicillin, and 100 µg mL^{-1} streptomycin under a humidified atmosphere of 95% of air and 5% of CO_2 at 37°C. The cells were passaged by using trypsinization, and the culture medium was replaced every other day. Cells at passage 5 were used for the next experiments.

2.8. Cell Viability Assay

The cytocompatibility of prepared iron oxide nanoparticles was evaluated *via* CCK-8 assay by culturing with HaCat cells and the cytotoxicity of DOX-loaded nanoparticles was assessed against A549 cells and HaCat cells, respectively. A certain amount of iron oxide nanoparticles was added into the cell medium, and no agglomeration phenomenon was observed under microscopy. The cell viability was quantitatively investigated using the CCK-8 assay. After removal of the culture media from cell culture plates, 300 µL fresh culture media and 30 µL CCK-8 kit solutions were immediately added and homogeneously mixed and then incubated for 4 h in a CO_2 incubator. Finally, 200 µL reaction solutions were transferred to a 96-well plate. The optical density at 450 nm (OD450) of each well was tested by a microplate reader (SpectraMax 190, Molecular Devices, USA), and the cell viability was calculated (the details are described in Electronic Supplementary Material). The fluorescent microscopy (Calcein AM/Ethidium Homodimer live/dead assay) was also used to investigate the morphology and proliferation of HaCat cells culturing with prepared nanoparticles on day 3.

2.9. Statistical Analysis

All data were given as mean ± SD (n = 5). Statistical analyses were performed using the SPSS software package. Levene's test was performed to determine the homogeneity of variance for all the data, and then Tamhane Post Hoc tests were performed for the comparison between different groups. The p-value of < 0.05 for 95% confidence was considered as statistically significant.

3. RESULTS AND DISCUSSION

The thermal decomposition of the iron-oleate complex was considered as an available method to fabricate large-scale uniform iron oxide nanoparticles. Then, the ligand exchange was used to obtain ligand-modified iron oxide nanoparticles, which were stable in the hydrophilic solvent [48]. Compared to the above synthesis method, a one-step precipitation method was employed here to synthesize hydrophilic nanoparticles (SPION). Fig. (**1a**) shows that the T-C-SPION was very stable while dispersed in water at room temperature (RT). Some black precipitations were observed without using a magnet while the reaction mixture was cooled down to RT for bare SPION, T-SPION, and C-SPION samples. After the magnet treatment and vacuum-drying, the T-C-SPION powder was obtained, as shown in Fig. (**1b**). Furthermore, the prepared dried T-C-SPION powder could be re-dispersed in Millipore water. Fig. (**1c**) shows that the T-C-SPION was uniformly dispersed in water instead of hexane while dispersed in water/hexane mixture, confirming T-C-SPION to be hydrophilic and stable in water.

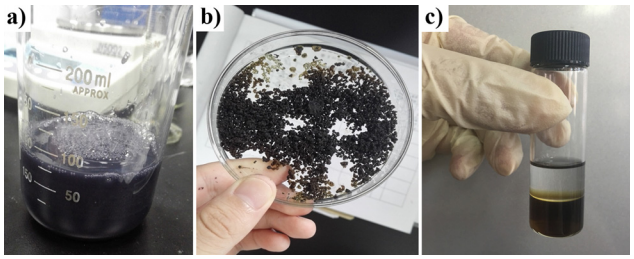

Fig. (1). Photographs of T-C-SPION dispersed in water after the reaction (**a**), and the large-scale T-C-SPION obtained after the magnet treatment and subsequent vacuum-drying (**b**). The stability of as-prepared T-C-SPION was tested by dispersing samples in water/hexane mixture; T-C-SPION was dispersed and stable in water instead of hexane (**c**). Photograph courtesy of Fang Zhang. (*A higher resolution / colour version of this figure is available in the electronic copy of the article*).

To better understand the crystalline structures of as-prepared SPION, XRD patterns of all samples were investigated, as shown in Fig. (**2a**). The results confirmed an inverse spinal structure of magnetite with the indices (2 1 1), (4 4 0), (3 1 1), (5 1 1), (4 0 0), and (4 2 2), which were also matched closely with the diffraction peaks of magnetite (JCPDS card, No. 77-1545). The sharp diffraction bands were indicative of the nano-crystalline nature of nanoparticles, and the sharpness of peaks indicated a higher order of crystallinity in the case of T-SPION and T-C-SPION, compared to bare SPION and C-SPION. Usually, the broad peak could be observed at an angle between 15-25°, mainly due to the amorphous polymeric coating on the surface of nanoparticles [38]. Here, the peak at $2\theta = 25°$ for T-SPION identified phytochemicals from green tea to be absorbed on SPION. After coating with tea molecules from green tea, like flavonoids and catechins, and citric acid, the excellent nanocrystalline property was displayed. Also, iron oxide and iron oxyhydroxide were observed for samples T-SPION and T-C-SPION [39].

FT-IR spectra of all kinds of SPIONs were performed to investigate the molecules capping on the SPION surface, and the results are shown in Fig. (**2b**). Compared to the reported FT-IR spectrum of citric acid, the peak at 1700 cm^{-1} was assignable to the C=O symmetric stretching from the COOH group of citric acid. However, such a peak shifted to the peak at 1600 cm^{-1} for T-C-SPION, as well as C-SPION, which was found to be consistent with the previous publication [27]. The peak that presented at 1710 cm^{-1} and the peak at about 1600 cm^{-1} appeared for C-SPION confirming citric acid molecules to be bound to the surface of SPION through chemisorption of carboxylate ions. For all samples, the low intense bands between 400 and 600 cm^{-1} were associated with the stretching and torsional vibration of the magnetite. Such as, the peak at 580 cm^{-1} was related to the vibration of the Fe-O bond, which matched well with the characteristics of iron oxide. Except for the bare SPION sample, the stretching of the O-H bond attached to the surface of SPION took place at about 3400 cm^{-1}. Between 1637 cm^{-1} and 1611 cm^{-1}, the absorption was dominated by the stretching vibration of the C=C aromatic ring contained mainly in the polyphenolic compounds. Moreover, the absorption bands at 1062 cm^{-1}

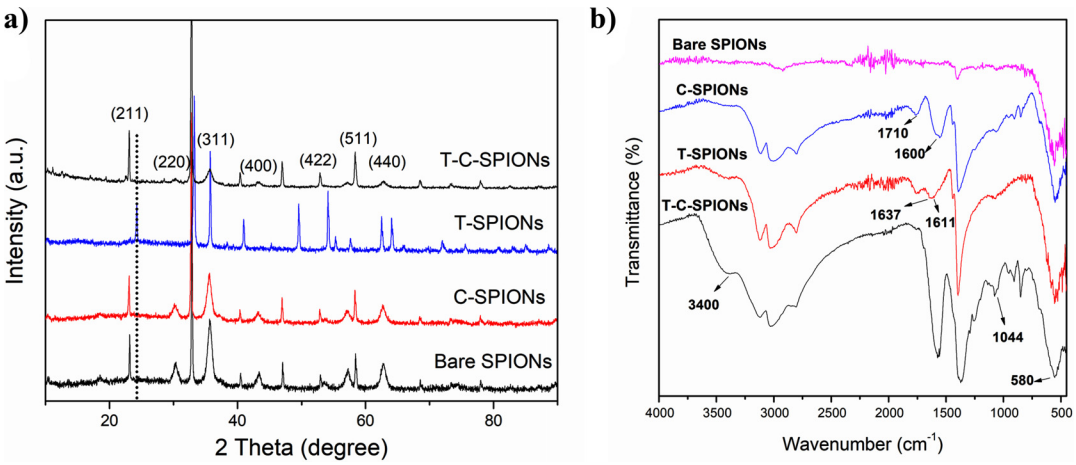

Fig. (2). XRD pattern (**a**) and FT-IR spectra (**b**) of bare SPION, C-SPION, T-SPION, and T-C-SPION powders. (*A higher resolution / colour version of this figure is available in the electronic copy of the article*).

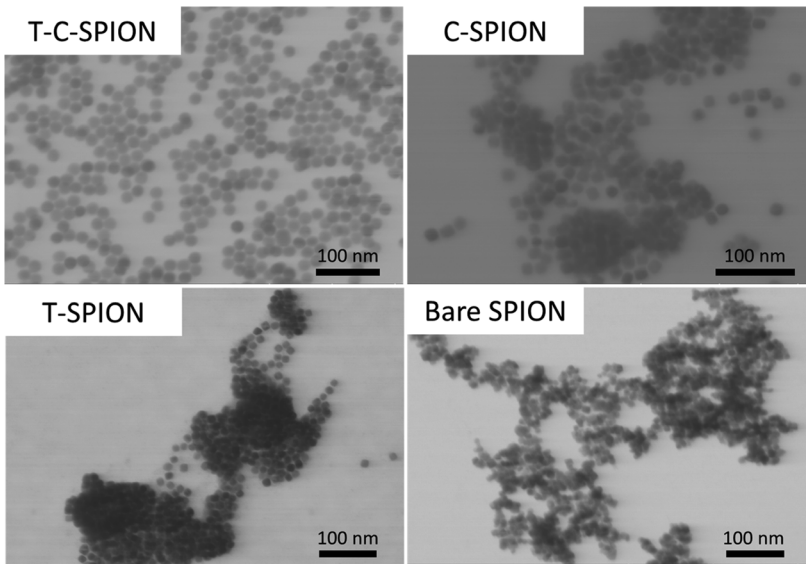

Fig. (3). TEM images of T-C-SPION, C-SPION, T-SPION, and bare SPION samples. (*A higher resolution / colour version of this figure is available in the electronic copy of the article*).

and 1044 cm^{-1} were characteristic of C-O-C, O-H. Uniquely, for T-C-SPION, 1367 cm^{-1} and 1361 cm^{-1} for C-N stretching vibration corresponded to aromatic amines, and 1040 cm^{-1} and 1048 cm^{-1} for C-N stretching vibration due to aliphatic amines [46]. Based on the above results, the bonding of some polyphenols and citric acid was confirmed. The main phytochemicals present in green tea consisting of catechins might be playing an essential role in SPION functionalization, and further as stabilizing agents, which was confirmed by the following TEM analysis [47].

TEM images of T-C-SPION, C-SPION, T-SPION, and bare SPION samples are displayed in Fig. (**3**). T-C-SPION exhibited a monodisperse spherical morphology with a diameter of 23.8 ± 0.8 nm. For T-SPION, C-SPION, and bare SPION samples, the aggregation phenomena were observed, and the average diameter was difficult to calculate by Fiji software. The balance of citric acid and polyphenols from green tea bonding on the surface of nanoparticles is related to the dispersity and stability of nanoparticles. Both polyphenols and citric acid coated on SPION are illustrated in Scheme **1**. The citrate-capped superparamagnetic iron oxide nanoparticles could be synthesized by a chemical precipitation method [23-27]. However, it is still challenging to obtain monodisperse nanoparticles using the above method. Also, the morphology of nanoparticles is easy-changeable, which depends on the reaction temperature, pH, and citric acid ratio, and so on. TEM results proved that citric acid in combination with green tea was a productive and facile method to synthesize the modified ion oxide nanoparticles with the excellent monodisperse property. Furthermore, it was reported that the diameter of iron oxide nanoparticles in the range of 15-40 nm showed excellent superparamagnetic properties [29, 30]. This confirmed that the saturation magnetization values of the iron oxide nanoparticles increased with the increase of grain sizes from 5.9 to 21.5 nm [49, 50]. Though the saturation magnetization value of T-C-SPION

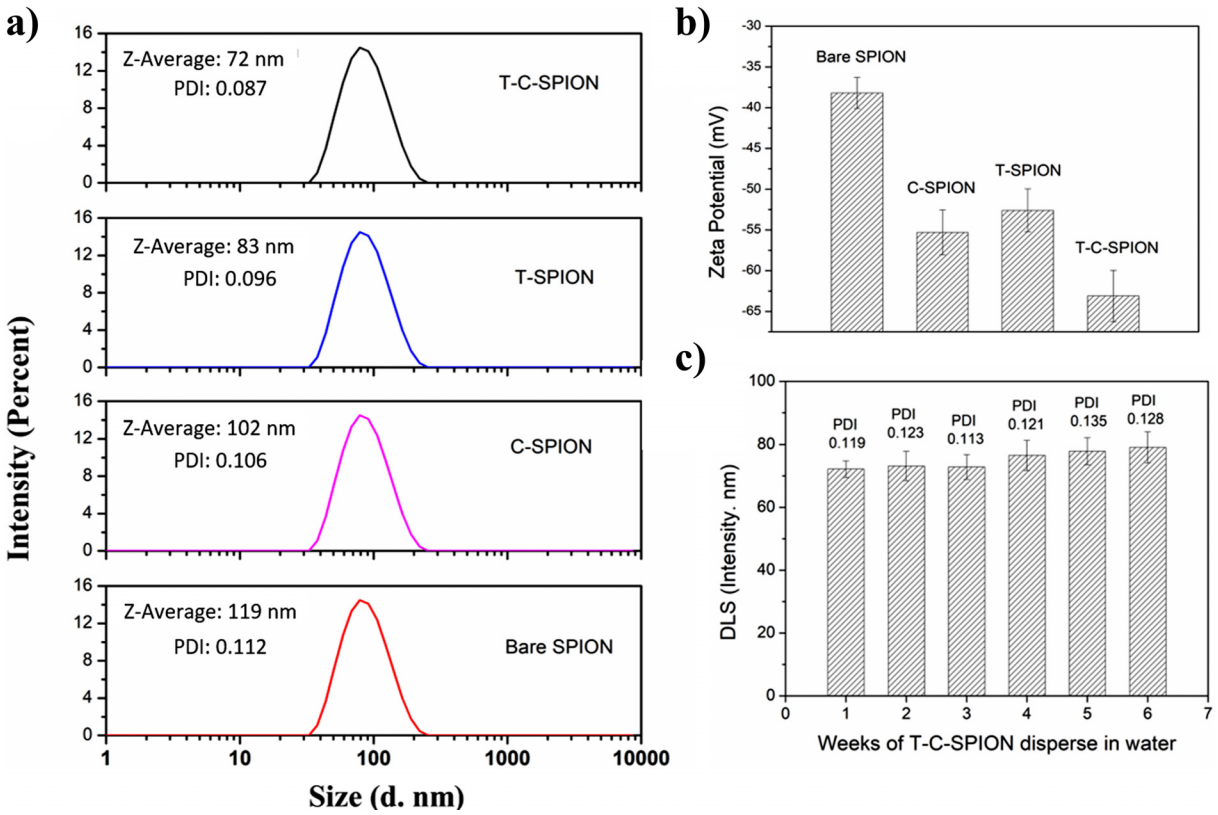

Fig. (4). The DLS analysis (**a**) and zeta potentials (**b**) of prepared T-C-SPION, C-SPION, T-SPION, and bare SPION nanoparticles dispersed in Millipore water. The diameter changes of T-C-SPION dispersed in water at 25 °C were monitored by DLS for 6 weeks (**c**). (*A higher resolution / colour version of this figure is available in the electronic copy of the article*).

was not tested yet here, it proposed that the obtained T-C-SPION possessed valuable magnetical property due to the range of diameter. Compared to polydisperse iron oxide nanoparticles, the monodisperse iron oxide nanoparticles showed much more stable physicochemical properties, such as stability in cell medium, higher drug loading efficiency, *etc.*, for biomedical applications [51, 52]. In this study, the monodisperse T-C-SPION was synthesized by one-step chemical coprecipitation using green tea leaf extract as the reaction solvent, and the balance of citric acid and polyphenols on the surface of SPION improved the stability in water and cell medium. Then, the hydrodynamic radius of nanoparticles and stability in water were evaluated next.

Due to Brownian motion in the solution and the subtle fluctuations of light intensity that occur at a resolution of a millisecond, the hydrodynamic radius of nanoparticles can be measured quickly and accurately *via* DLS. Here, DLS was applied to measure the size distribution of prepared nanoparticles in Millipore water (Fig. **4a**), in which the pH of water nanoparticles dispersed was checked (around 7) before testing. Fig. (**4a**) indicates that the obtained nanoparticles had a narrow size distribution. As the aggregation was alleviated, the hydrodynamic size distribution decreased to 72 nm (T-C-SPION), 83 nm (T-SPION), and 102 nm (C-SPION), compared to bare SPION (119 nm). Also, due to the citric acid or/and polyphenols capped on iron oxide nanoparticles, T-C-SPION showed the smallest hydrodynamic radius. Compared to the diameter of dried nanoparticles, the average diameter calculated by DLS was larger. Also, the zeta potentials of the prepared nanoparticles in water were tested to evaluate their stability, as shown in Fig. (**4b**). It is known that zeta potential is an essential indicator of colloidal dispersion stability *via* measuring mutual repulsion or attraction strength between particles, and the higher absolute value of the zeta potential (positive or negative) indicates much more stability of nanoparticles solution. The zeta potentials of bare SPION, C-SPION, T-SPION, and T-C-SPION are -33, -51, -48, and -58 mV, respectively. Without modification, the zeta potential value of bare SPION was close to the range of ±10 ~ ± 30, proving that the bare SPION became unstable in water. After coating with citric acid or/and polyphenols on SPION, the nanoparticles were generally more stable due to the repelling forces amongst each other [20, 53], confirming that the colloidal stability of SPION was improved. T-C-SPION showed the best colloidal stability compared to T-SPION and C-SPION. Moreover, in consideration of potential application feasibility, the stability of T-C-SPION in water during the store process was evaluated. The nanoparticles dispersed in water were stored in the refrigerator at 4°C for 6 weeks. The average diameter of T-C-SPION showed a very slight increase with increasing storage weeks, as shown in Fig. (**4c**).

Before the *in vitro* test, the stability of nanoparticles in the cell medium needs to be evaluated first. Due to that, the Dulbecco's modified Eagle's medium was the main component in the cell medium during the cell culture, so Dulbecco's modified Eagle's medium was used as a dispersion medium in this paper. According to the DLS results (Fig. **S1**,

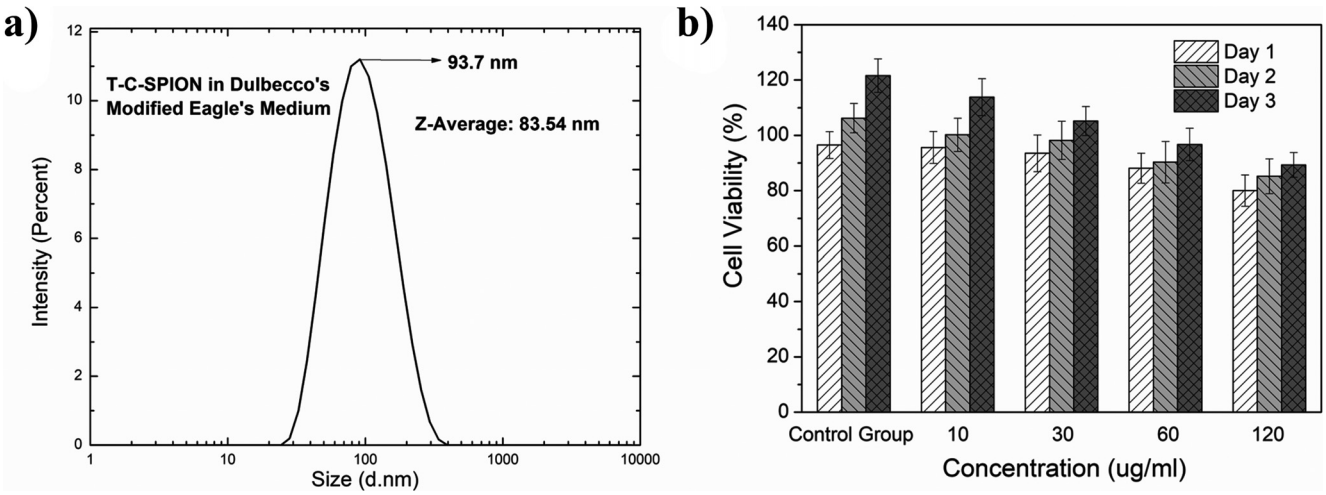

Fig. (5). (**a**) Diameter distribution of T-C-SPION dispersed in Dulbecco's modified Eagle's medium by DLS analysis. (**b**) *In vitro* cytotoxicity of T-C-SPION with different iron concentrations after incubation with HaCat cells for a different number of days (1~3 days), without adding T-C-SPION as Control Group. (*A higher resolution / colour version of this figure is available in the electronic copy of the article*).

Electronic Supplementary Material), the multi-peaks were observed for samples bare SPION, C-SPION, and T-SPION, proving that the above nanoparticles were not stable while dispersing in cell medium. The stability of T-C-SPION in cell medium is displayed in Fig. (**5a**). It was surprising that the average diameter of T-C-SPION in cell medium increased from 72.01 nm to 83.54 nm compared to T-C-SPION dispersed in water, which proved that the T-C-SPION was stable without aggregation in Dulbecco's modified Eagle's medium. The obtained biological evaluation demonstrated that the obtained iron oxide nanoparticles had colloidal stability, which is potentially applied in biomedical fields [54]. Next, the obtained nanoparticles were used for the next *in vitro* cytocompatibility. Before that, the iron concentrations of nanoparticles were measured by AAS using the standard curve of iron absorption (Fig. **S2**, Electronic Supplementary Material). Then, the cytocompatibility of nanoparticles was evaluated by CCK-8 assay by culturing with HaCat cells using different iron concentrations from 10 to 120 ug/mL, and the result for T-C-SPION is shown in Fig. (**5b**). The HaCat cell viability increased with the decrease in iron concentration. However, the cell viabilities increased to 90%, at least for all T-C-SPION samples. For bare SPION, C-SPION, T-SPION samples, the cell viabilities decreased compared to that of T-C-SPION. Some research data displayed that the cell viability reduced to 50% at the iron concentrations of 300-500 ug/mL, mainly because intracellular reactive oxygen species (ROS) are generated when there is an exposure to a higher level of nanoparticles, leading to cell injury and death [55].

On the other hand, the morphology of HaCat cells was observed using Calcein AM/Ethidium Homodimer staining after culturing with prepared nanoparticles on day 3; the fluorescence images of HaCat cells are shown in Fig. (**6**). The live cells are represented by green-stained color, and dead cells are represented by red-stained color. Compared to the control group, it was apparent that the number of live cells in

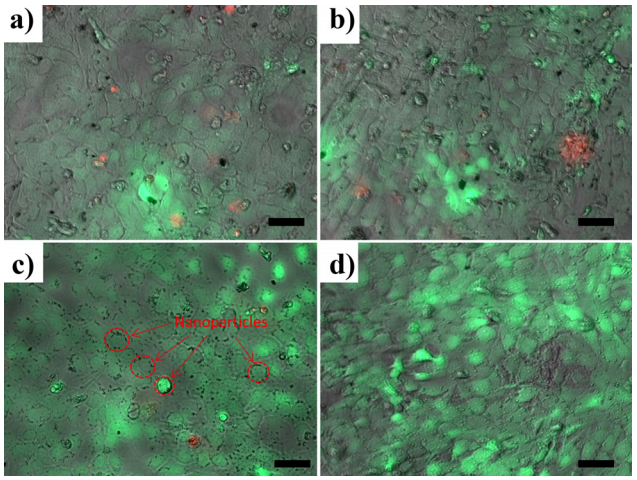

Fig. (6). Fluorescence images of HaCat cells cultured with T-SPION (**a**), C-SPION (**b**), and T-C-SPION (**c**) at day 3, with untreated group as Control Group (**d**), Calcein AM/Ethidium Homodimer live/dead assay, scale bar: 50 μm. (*A higher resolution / colour version of this figure is available in the electronic copy of the article*).

incubation with iron oxide nanoparticles decreased. Moreover, the number of live cells in incubation with T-C-SPION was relatively higher than that of T-SPION and C-SPION, which corresponded with CCK-8 results. Also, it was observed that some nanoparticles accumulated near the surface of cells, which further led to the deformation of the cells to a spherical shape compared to the control group [56].

The molecules capped on the surface of iron oxide nanoparticles could provide drug loading sites for DOX [57]. The DOX E_{encaps} of DOX-loaded bare SPION, C-SPION, T-SPION, and T-C-SPION were measured, as shown in Fig. (**7a**). Due to electrostatic interactions and hydrogen bonds, the catechins and citric acid capped on SPION could

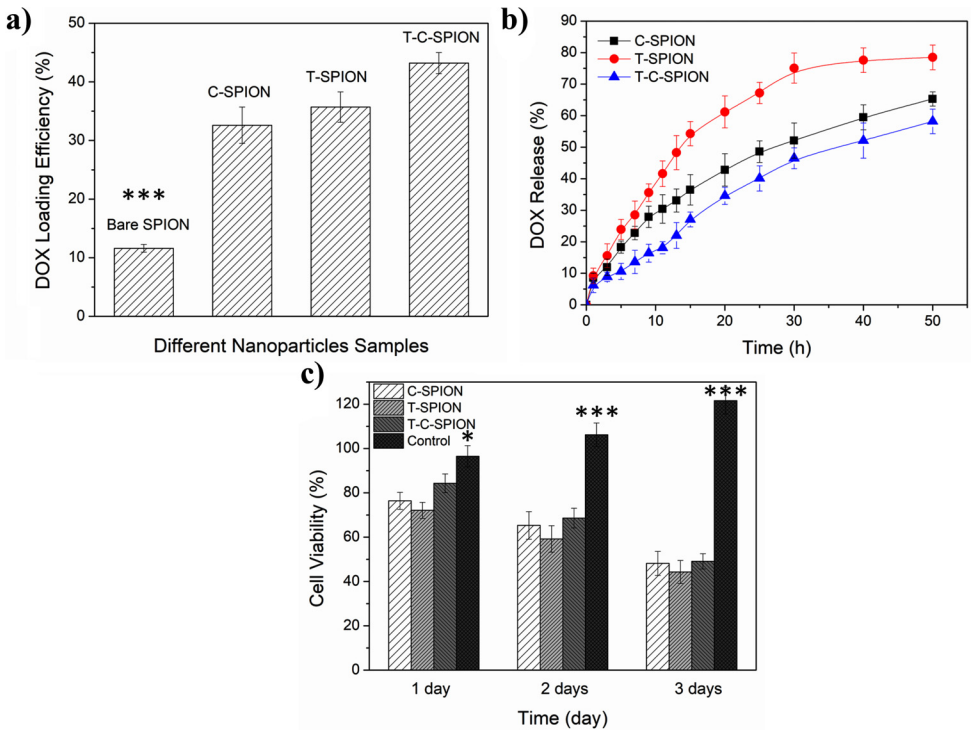

Fig. (7). (**a**) DOX E_{encaps} of bare SPION, C-SPION, T-SPION, and T-C-SPION, and (**b**) *in vitro* DOX release profiles of all kinds of DOX-loaded nanoparticles in PBS, and (**c**) *in vitro* cytotoxicity of DOX-loaded C-SPION, T-SPION, and T-C-SPION after incubation with A549 cells at different days; iron concentration for all samples was 30 μg/mL. (*A higher resolution / colour version of this figure is available in the electronic copy of the article*).

facilitate DOX loading (Schemes **1** and **2**). DOX E_{encaps} of T-C-SPION (43.2 ± 1.8 %) was higher than that of T-SPION and C-SPION. The release profiles of DOX from DOX-loaded nanoparticles in PBS were tested, as shown in Fig. (**7b**). The DOX-loaded T-SPION showed a biphasic release pattern consisting of a relatively rapid initial release which then followed the sustained release. However, DOX-loaded T-C-SPION performed a different release pattern with a relatively slow initial release first, then followed by a sustained release. Moreover, the release profile curve of DOX for DOX-loaded C-SPION was in between them. The different release profiles were mainly due to the hydrogen bond interactions between DOX and catechins and/or citric acid; also, the losses in DOX-Fe^{3+} chelation [58], and the possible loading mechanism for T-C-SPION are shown in Scheme **2**.

The sustained release was beneficial for tumor cell killing, and the CCK-8 assay was used to investigate the cytotoxicity of DOX loaded nanoparticles against A549 cells (Fig. **S3**, Electronic Supplementary Material). The DOX-loaded nanoparticles with a faster DOX release rate exhibited lower cell viability and *vice versa*. Previous data confirmed that DOX could diffuse into cells rapidly, and nanoparticles were endocytosed to enter the cells with a lag period [59]. In this work, it was apparent that the prepared nanoparticles, such as T-C-SPION, gathered near cells on day 3, which facilitated the endocytosis of cells. The iron oxide nanoparticles with higher DOX E_{encaps} showed superiority in overall effectiveness as a drug delivery agent, and a sustained release maintained sufficient drug concentrations at the tumor site with reducing dosing frequency and side effects.

CONCLUSION

In summary, the iron oxide nanoparticles could be facilely synthesized using green tea extract with citric acid. The prepared T-C-SPION was spherical with a diameter of 23.8 ± 0.8 nm; also, it was water-dispersible and stable in water, even stored in water for 6 weeks. Next, the CCK-8 assay proved that T-C-SPION possessed a good cytocompatibility while the iron concentration was in a range of 10 to 120 ug/mL. The anti-cancer drug DOX could be loaded on prepared nanoparticles and displayed a sustained release profile. Finally, as-prepared T-C-SPION with good cytotoxicity and good E_{encaps} of DOX suggested that developed iron oxide nanoparticles *via* green tea extract could be applied as a potential drug carrier for cancer chemotherapy.

AUTHORS' CONTRIBUTIONS

Lei Nie: Conceptualization, Methodology, Validation, Formal analysis, Investigation, Writing-Review and Editing, Supervision, Project administration, Funding acquisition Chenlei Cai: Investigation, Data Curation, Writing-Original Draft, Writing-Review and Editing Meng Sun: Writing-Original Draft, Writing-Review and Editing Fang Zhang: Formal analysis, Investigation, Writing-Original Draft Lingyun Zheng: Formal analysis, Software Qi Peng: Formal analysis, Investigation Amin Shavandi: Conceptualization,

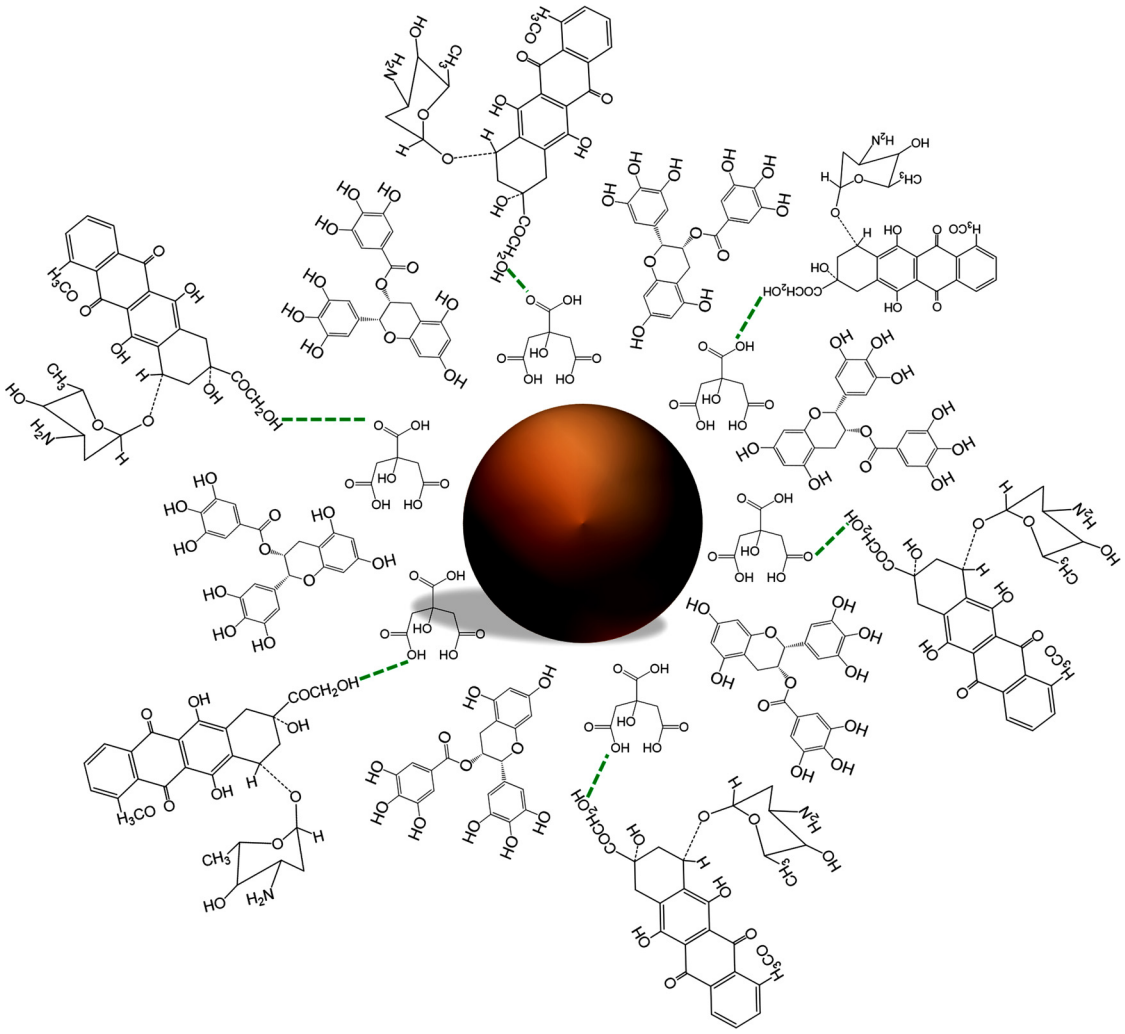

Scheme 2. The mechanism of DOX loaded on prepared T-C-SPION. (*A higher resolution / colour version of this figure is available in the electronic copy of the article*).

Writing-Review and Editing, Supervision Shoufeng Yang: Writing-Review and Editing, Supervision.

ETHICS APPROVAL AND CONSENT TO PARTICIPATE

Not applicable.

HUMAN AND ANIMAL RIGHTS

No animals/humans were used for studies that are the basis of this research.

CONSENT FOR PUBLICATION

Not applicable.

AVAILABILITY OF DATA AND MATERIALS

All data generated or analyzed in this work are included in the published article and its Electronic Supplementary Materials and are available from the corresponding authors on reasonable request.

FUNDING

This research was supported by the National Natural Science Foundation of China (31700840) and the Zhejiang Natural Science Foundation of China (LQ16E030002).

CONFLICT OF INTEREST

The authors declare no conflict of interest, financial or otherwise.

ACKNOWLEDGEMENTS

We appreciated Dr. Jilai Cui and Miss Jie Zhou from XYNU working in related tea research areas for their valuable suggestions. The authors would like to acknowledge the Nanhu Scholars Program for Young Scholars of XYNU.

SUPPLEMENTARY MATERIAL

Supplementary material is available on the publisher's website along with the published article.

REFERENCES

[1] Nune, S.K.; Chanda, N.; Shukla, R.; Katti, K.; Kulkarni, R.R.; Thilakavathi, S.; Mekapothula, S.; Kannan, R.; Katti, K.V. Green nanotechnology from tea: Phytochemicals in tea as building blocks for production of biocompatible gold nanoparticles. *J. Mater. Chem.,* **2009**, *19*(19), 2912-2920. http://dx.doi.org/10.1039/b822015h PMID: 20161162

[2] Hamer, M. The beneficial effects of tea on immune function and inflammation: a review of evidence from *in vitro*, animal, and human research. *Nutr. Res.,* **2007**, *27*(7), 373-379. http://dx.doi.org/10.1016/j.nutres.2007.05.008

[3] Yang, C.S.; Lambert, J.D.; Ju, J.; Lu, G.; Sang, S. Tea and cancer prevention: molecular mechanisms and human relevance. *Toxicol. Appl. Pharmacol.,* **2007**, *224*(3), 265-273. http://dx.doi.org/10.1016/j.taap.2006.11.024 PMID: 17234229

[4] Hodgson, J.M. Effects of tea and tea flavonoids on endothelial function and blood pressure: a brief review. *Clin. Exp. Pharmacol. Physiol.,* **2006**, *33*(9), 838-841. http://dx.doi.org/10.1111/j.1440-1681.2006.04450.x PMID: 16922817

[5] Cabrera, C.; Artacho, R.; Giménez, R. Beneficial effects of green tea--a review. *J. Am. Coll. Nutr.,* **2006**, *25*(2), 79-99. http://dx.doi.org/10.1080/07315724.2006.10719518 PMID: 16582024

[6] Chacko, S.M.; Thambi, P.T.; Kuttan, R.; Nishigaki, I. Beneficial effects of green tea: a literature review. *Chin. Med.,* **2010**, *5*(1), 13. http://dx.doi.org/10.1186/1749-8546-5-13 PMID: 20370896

[7] Jankun, J.; Selman, S.H.; Swiercz, R.; Skrzypczak-Jankun, E. Why drinking green tea could prevent cancer. *Nature,* **1997**, *387*(6633), 561. http://dx.doi.org/10.1038/42381 PMID: 9177339

[8] Fujiki, H.; Sueoka, E.; Watanabe, T.; Suganuma, M. Primary cancer prevention by green tea, and tertiary cancer prevention by the combination of green tea catechins and anticancer compounds. *J. Cancer Prev.,* **2015**, *20*(1), 1-4. http://dx.doi.org/10.15430/JCP.2015.20.1.1 PMID: 25853098

[9] Miller, K.D.; Siegel, R.L.; Lin, C.C.; Mariotto, A.B.; Kramer, J.L.; Rowland, J.H.; Stein, K.D.; Alteri, R.; Jemal, A. Cancer treatment and survivorship statistics, 2016. *CA Cancer J. Clin.,* **2016**, *66*(4), 271-289. http://dx.doi.org/10.3322/caac.21349 PMID: 27253694

[10] Vanneman, M.; Dranoff, G. Combining immunotherapy and targeted therapies in cancer treatment. *Nat. Rev. Cancer,* **2012**, *12*(4), 237-251. http://dx.doi.org/10.1038/nrc3237 PMID: 22437869

[11] Fukuhara, H.; Ino, Y.; Todo, T. Oncolytic virus therapy: A new era of cancer treatment at dawn. *Cancer Sci.,* **2016**, *107*(10), 1373-1379. http://dx.doi.org/10.1111/cas.13027 PMID: 27486853

[12] Kennedy, L.C.; Bickford, L.R.; Lewinski, N.A.; Coughlin, A.J.; Hu, Y.; Day, E.S.; West, J.L.; Drezek, R.A. A new era for cancer treatment: gold-nanoparticle-mediated thermal therapies. *Small,* **2011**, *7*(2), 169-183. http://dx.doi.org/10.1002/smll.201000134 PMID: 21213377

[13] Chen, J.; Glaus, C.; Laforest, R.; Zhang, Q.; Yang, M.; Gidding, M.; Welch, M.J.; Xia, Y. Gold nanocages as photothermal transducers for cancer treatment. *Small,* **2010**, *6*(7), 811-817. http://dx.doi.org/10.1002/smll.200902216 PMID: 20225187

[14] Davis, M.E.; Chen, Z.G.; Shin, D.M. Nanoparticle therapeutics: an emerging treatment modality for cancer. *Nat. Rev. Drug Discov.,* **2008**, *7*(9), 771-782. http://dx.doi.org/10.1038/nrd2614 PMID: 18758474

[15] Gabizon, A.; Shmeeda, H.; Barenholz, Y. Pharmacokinetics of pegylated liposomal Doxorubicin: review of animal and human studies. *Clin. Pharmacokinet.,* **2003**, *42*(5), 419-436. http://dx.doi.org/10.2165/00003088-200342050-00002 PMID: 12739982

[16] Zhu, L.; Wang, D.; Wei, X.; Zhu, X.; Li, J.; Tu, C.; Su, Y.; Wu, J.; Zhu, B.; Yan, D. Multifunctional pH-sensitive superparamagnetic iron-oxide nanocomposites for targeted drug delivery and MR imaging. *J. Control Release,* **2013**, *169*(3), 228-238. http://dx.doi.org/10.1016/j.jconrel.2013.02.015 PMID: 23485450

[17] Zanganeh, S.; Hutter, G.; Spitler, R.; Lenkov, O.; Mahmoudi, M.; Shaw, A.; Pajarinen, J.S.; Nejadnik, H.; Goodman, S.; Moseley, M.; Coussens, L.M.; Daldrup-Link, H.E. Iron oxide nanoparticles inhibit tumour growth by inducing pro-inflammatory macrophage polarization in tumour tissues. *Nat. Nanotechnol.,* **2016**, *11*(11), 986-994. http://dx.doi.org/10.1038/nnano.2016.168 PMID: 27668795

[18] Sakulkhu, U.; Mahmoudi, M.; Maurizi, L.; Coullerez, G.; Hofmann-Amtenbrink, M.; Vries, M.; Motazacker, M.; Rezaee, F.; Hofmann, H. Significance of surface charge and shell material of superparamagnetic iron oxide nanoparticle (SPION) based core/shell nanoparticles on the composition of the protein corona. *Biomater. Sci.,* **2015**, *3*(2), 265-278. http://dx.doi.org/10.1039/C4BM00264D PMID: 26218117

[19] Espinosa, A.; Di Corato, R.; Kolosnjaj-Tabi, J.; Flaud, P.; Pellegrino, T.; Wilhelm, C. Duality of iron oxide nanoparticles in cancer therapy: Amplification of heating efficiency by magnetic hyperthermia and photothermal bimodal treatment. *ACS Nano,* **2016**, *10*(2), 2436-2446. http://dx.doi.org/10.1021/acsnano.5b07249 PMID: 26766814

[20] Mahmoudi, M.; Sahraian, M.A.; Shokrgozar, M.A.; Laurent, S. Superparamagnetic iron oxide nanoparticles: promises for diagnosis and treatment of multiple sclerosis. *ACS Chem. Neurosci.,* **2011**, *2*(3), 118-140. http://dx.doi.org/10.1021/cn100100e PMID: 22778862

[21] Li, W.; Tutton, S.; Vu, A.T.; Pierchala, L.; Li, B.S.Y.; Lewis, J.M.; Prasad, P.V.; Edelman, R.R. First-pass contrast-enhanced magnetic resonance angiography in humans using ferumoxytol, a novel ultrasmall superparamagnetic iron oxide (USPIO)-based blood pool agent. *J. Magn. Reson. Imaging,* **2005**, *21*(1), 46-52. http://dx.doi.org/10.1002/jmri.20235 PMID: 15611942

[22] Szekeres, M.; Tóth, I.Y.; Illés, E.; Hajdú, A.; Zupkó, I.; Farkas, K.; Oszlánczi, G.; Tiszlavicz, L.; Tombácz, E. Chemical and colloidal stability of carboxylated core-shell magnetite nanoparticles designed for biomedical applications. *Int. J. Mol. Sci.,* **2013**, *14*(7), 14550-14574. http://dx.doi.org/10.3390/ijms140714550 PMID: 23857054

[23] Thanh, N.T.K.; Maclean, N.; Mahiddine, S. Mechanisms of nucleation and growth of nanoparticles in solution. *Chem. Rev.,* **2014**, *114*(15), 7610-7630. http://dx.doi.org/10.1021/cr400544s PMID: 25003956

[24] Gul, S.; Khan, S.B.; Rehman, I.U.; Khan, M.A.; Khan, M.I. A comprehensive review of magnetic nanomaterials modern day theranostics. *Front. Mater.,* **2019**, *6*, 179. http://dx.doi.org/10.3389/fmats.2019.00179

[25] Roth, H-C.; Schwaminger, S.P.; Schindler, M.; Wagner, F.E.; Berensmeier, S. Influencing factors in the CO-precipitation process of superparamagnetic iron oxide nano particles: A model based study. *J. Magn. Magn. Mater.,* **2015**, *377*, 81-89. http://dx.doi.org/10.1016/j.jmmm.2014.10.074

[26] Li, L.; Mak, K.Y.; Leung, C.W.; Chan, K.Y.; Chan, W.K.; Zhong, W.; Pong, P.W.T. Effect of synthesis conditions on the properties of citric-acid coated iron oxide nanoparticles. *Microelectron. Eng.,* **2013**, *110*, 329-334. http://dx.doi.org/10.1016/j.mee.2013.02.045

[27] Răcuciu, M.; Creangă, D.E.; Airinei, A. Citric-acid-coated magnetite nanoparticles for biological applications. *Eur. Phys J.E Soft Matter,* **2006**, *21*(2), 117-121. http://dx.doi.org/10.1140/epje/i2006-10051-y PMID: 17180642

[28] Laurent, S.; Forge, D.; Port, M.; Roch, A.; Robic, C.; Vander Elst, L.; Muller, R.N. Magnetic iron oxide nanoparticles: synthesis, stabilization, vectorization, physicochemical characterizations, and biological applications. *Chem. Rev.,* **2008**, *108*(6), 2064-2110. http://dx.doi.org/10.1021/cr068445e PMID: 18543879

[29] Li, S.; Zhang, T.; Tang, R.; Qiu, H.; Wang, C.; Zhou, Z. Solvothermal synthesis and characterization of monodisperse superparamagnetic iron oxide nanoparticles. *J. Magn. Magn. Mater.,* **2015**, *379*, 226-231. http://dx.doi.org/10.1016/j.jmmm.2014.12.054

[30] Park, J.; Lee, E.; Hwang, N-M.; Kang, M.; Kim, S.C.; Hwang, Y.; Park, J-G.; Noh, H-J.; Kim, J-Y.; Park, J-H.; Hyeon, T. One-

nanometer-scale size-controlled synthesis of monodisperse magnetic iron oxide nanoparticles. *Angew. Chem. Int. Ed. Engl.,* **2005**, *44*(19), 2873-2877.
http://dx.doi.org/10.1002/anie.200461665 PMID: 15798989

[31] Park, J.; An, K.; Hwang, Y.; Park, J-G.; Noh, H-J.; Kim, J-Y.; Park, J-H.; Hwang, N-M.; Hyeon, T. Ultra-large-scale syntheses of monodisperse nanocrystals. *Nat. Mater.,* **2004**, *3*(12), 891-895.
http://dx.doi.org/10.1038/nmat1251 PMID: 15568032

[32] Hufschmid, R.; Arami, H.; Ferguson, R.M.; Gonzales, M.; Teeman, E.; Brush, L.N.; Browning, N.D.; Krishnan, K.M. Synthesis of phase-pure and monodisperse iron oxide nanoparticles by thermal decomposition. *Nanoscale,* **2015**, *7*(25), 11142-11154.
http://dx.doi.org/10.1039/C5NR01651G PMID: 26059262

[33] Korpany, K.V.; Mottillo, C.; Bachelder, J.; Cross, S.N.; Dong, P.; Trudel, S.; Friščić, T.; Blum, A.S. One-step ligand exchange and switching from hydrophobic to water-stable hydrophilic superparamagnetic iron oxide nanoparticles by mechanochemical milling. *Chem. Commun. (Camb.),* **2016**, *52*(14), 3054-3057.
http://dx.doi.org/10.1039/C5CC07107K PMID: 26794225

[34] Bixner, O.; Lassenberger, A.; Baurecht, D.; Reimhult, E. Complete exchange of the hydrophobic dispersant shell on monodisperse superparamagnetic iron oxide nanoparticles. *Langmuir,* **2015**, *31*(33), 9198-9204.
http://dx.doi.org/10.1021/acs.langmuir.5b01833 PMID: 26226071

[35] Illés, E.; Szekeres, M.; Tóth, I.Y.; Szabó, Á.; Iván, B.; Turcu, R.; Vékás, L.; Zupkó, I.; Jaics, G.; Tombácz, E. Multifunctional PEG-carboxylate copolymer coated superparamagnetic iron oxide nanoparticles for biomedical application. *J. Magn. Magn. Mater.,* **2018**, *451*, 710-720.
http://dx.doi.org/10.1016/j.jmmm.2017.11.122

[36] Karimzadeh, I.; Aghazadeh, M.; Doroudi, T.; Ganjali, M.R.; Kolivand, P.H. Superparamagnetic iron oxide (Fe_3O_4) nanoparticles coated with PEG/PEI for biomedical applications: A facile and scalable preparation route based on the cathodic electrochemical deposition method. *Adv. Phys. Chem.,* **2017**, *2017,* 9437487.
http://dx.doi.org/10.1155/2017/9437487

[37] Shavandi, A.; Saeedi, P.; Ali, M.A.; Jalalvandi, E. Green synthesis of polysaccharide-based inorganic nanoparticles and biomedical aspects. *Functional Polysaccharides for Biomedical Applications*; Maiti, S.; Jana, S., Eds.; Woodhead Publishing, **2019**, pp. 267-304.
http://dx.doi.org/10.1016/B978-0-08-102555-0.00008-X

[38] Asadi, H.; Khoee, S.; Deckers, R. Polymer-grafted superparamagnetic iron oxide nanoparticles as a potential stable system for magnetic resonance imaging and doxorubicin delivery. *RSC Advances,* **2016**, *6*(87), 83963-83972.
http://dx.doi.org/10.1039/C6RA20398A

[39] Hoag, G.E.; Collins, J.B.; Holcomb, J.L.; Hoag, J.R.; Nadagouda, M.N.; Varma, R.S. Degradation of bromothymol blue by 'greener' nano-scale zero-valent iron synthesized using tea polyphenols. *J. Mater. Chem.,* **2009**, *19*(45), 8671-8677.
http://dx.doi.org/10.1039/b909148c

[40] Tran, T.T-D.; Van Vo, T.; Tran, P.H-L. Design of iron oxide nanoparticles decorated oleic acid and bovine serum albumin for drug delivery. *Chem. Eng. Res. Des.,* **2015**, *94*, 112-118.
http://dx.doi.org/10.1016/j.cherd.2014.12.016

[41] Saraswathy, A.; Nazeer, S.S.; Jeevan, M.; Nimi, N.; Arumugam, S.; Harikrishnan, V.S.; Varma, P.R.H.; Jayasree, R.S. Citrate coated iron oxide nanoparticles with enhanced relaxivity for *in vivo* magnetic resonance imaging of liver fibrosis. *Colloids Surf. B Biointerfaces,* **2014**, *117*, 216-224.
http://dx.doi.org/10.1016/j.colsurfb.2014.02.034 PMID: 24646453

[42] Shahwan, T.; Abu Sirriah, S.; Nairat, M.; Boyacı, E.; Eroğlu, A.E.; Scott, T.B.; Hallam, K.R. Green synthesis of iron nanoparticles and their application as a fenton-like catalyst for the degradation of aqueous cationic and anionic dyes. *Chem. Eng. J.,* **2011**, *172*(1), 258-266.
http://dx.doi.org/10.1016/j.cej.2011.05.103

[43] Shavandi, A.; Bekhit, A.E.A.; Saeedi, P.; Izadifar, Z.; Bekhit, A.A.; Khademhosseini, A. Polyphenol uses in biomaterials engineering. *Biomaterials,* **2018**, *167*, 91-106.
http://dx.doi.org/10.1016/j.biomaterials.2018.03.018 PMID: 29567389

[44] Huang, L.; Weng, X.; Chen, Z.; Megharaj, M.; Naidu, R. Green synthesis of iron nanoparticles by various tea extracts: comparative study of the reactivity. *Spectrochim. Acta A Mol. Biomol. Spectrosc.,* **2014**, *130*, 295-301.
http://dx.doi.org/10.1016/j.saa.2014.04.037 PMID: 24793479

[45] Wang, T.; Lin, J.; Chen, Z.; Megharaj, M.; Naidu, R. green synthesized iron nanoparticles by green tea and eucalyptus leaves extracts used for removal of nitrate in aqueous solution. *J. Clean. Prod.,* **2014**, *83*, 413-419.
http://dx.doi.org/10.1016/j.jclepro.2014.07.006

[46] Das, R.K.; Borthakur, B.B.; Bora, U. Green synthesis of gold nanoparticles using ethanolic leaf extract of *Centella asiatica. Mater. Lett.,* **2010**, *64*(13), 1445-1447.
http://dx.doi.org/10.1016/j.matlet.2010.03.051

[47] Quinto, C.A.; Mohindra, P.; Tong, S.; Bao, G. Multifunctional superparamagnetic iron oxide nanoparticles for combined chemotherapy and hyperthermia cancer treatment. *Nanoscale,* **2015**, *7*(29), 12728-12736.
http://dx.doi.org/10.1039/C5NR02718G PMID: 26154916

[48] Kim, B.H.; Lee, N.; Kim, H.; An, K.; Park, Y.I.; Choi, Y.; Shin, K.; Lee, Y.; Kwon, S.G.; Na, H.B.; Park, J-G.; Ahn, T-Y.; Kim, Y-W.; Moon, W.K.; Choi, S.H.; Hyeon, T. Large-scale synthesis of uniform and extremely small-sized iron oxide nanoparticles for high-resolution T1 magnetic resonance imaging contrast agents. *J. Am. Chem. Soc.,* **2011**, *133*(32), 12624-12631.
http://dx.doi.org/10.1021/ja203340u PMID: 21744804

[49] Pereira, C.; Pereira, A.M.; Fernandes, C.; Rocha, M.; Mendes, R.; Fernández-García, M.P.; Guedes, A.; Tavares, P.B.; Grenèche, J-M.; Araújo, J.P.; Freire, C. Superparamagnetic MFe_2O_4 (M = Fe, Co, Mn) nanoparticles: Tuning the particle size and magnetic properties through a novel one-step coprecipitation route. *Chem. Mater.,* **2012**, *24*(8), 1496-1504.
http://dx.doi.org/10.1021/cm300301c

[50] Xuan, S.; Wang, Y-X.J.; Yu, J.C.; Leung, K.C-F. Tuning the grain size and particle size of superparamagnetic Fe_3O_4 microparticles. *Chem. Mater.,* **2009**, *21*(21), 5079-5087.
http://dx.doi.org/10.1021/cm901618m

[51] Patsula, V.; Moskvin, M.; Dutz, S.; Horák, D. Size-dependent magnetic properties of iron oxide nanoparticles. *J. Phys. Chem. Solids,* **2016**, *88*, 24-30.
http://dx.doi.org/10.1016/j.jpcs.2015.09.008

[52] Rezayan, A.H.; Mousavi, M.; Kheirjou, S.; Amoabediny, G.; Ardestani, M.S.; Mohammadnejad, J. Monodisperse magnetite (Fe_3O_4) nanoparticles modified with water soluble polymers for the diagnosis of breast cancer by MRI method. *J. Magn. Magn. Mater.,* **2016**, *420*, 210-217.
http://dx.doi.org/10.1016/j.jmmm.2016.07.003

[53] Korpany, K.V.; Habib, F.; Murugesu, M.; Blum, A.S. Stable water-soluble iron oxide nanoparticles using tiron. *Mater. Chem. Phys.,* **2013**, *138*(1), 29-37.
http://dx.doi.org/10.1016/j.matchemphys.2012.10.015

[54] Petri-Fink, A.; Steitz, B.; Finka, A.; Salaklang, J.; Hofmann, H. Effect of cell media on polymer coated superparamagnetic iron oxide nanoparticles (SPIONs): colloidal stability, cytotoxicity, and cellular uptake studies. *Eur. J. Pharm. Biopharm.,* **2008**, *68*(1), 129-137.
http://dx.doi.org/10.1016/j.ejpb.2007.02.024 PMID: 17881203

[55] Naqvi, S.; Samim, M.; Abdin, M.; Ahmed, F.J.; Maitra, A.; Prashant, C.; Dinda, A.K. Concentration-dependent toxicity of iron oxide nanoparticles mediated by increased oxidative stress. *Int. J. Nanomedicine,* **2010**, *5*, 983-989.
http://dx.doi.org/10.2147/IJN.S13244 PMID: 21187917

[56] Mahmoudi, M.; Simchi, A.; Milani, A.S.; Stroeve, P. Cell toxicity of superparamagnetic iron oxide nanoparticles. *J. Colloid Interface Sci.,* **2009**, *336*(2), 510-518.
http://dx.doi.org/10.1016/j.jcis.2009.04.046 PMID: 19476952

[57] Lee, N.; Yoo, D.; Ling, D.; Cho, M.H.; Hyeon, T.; Cheon, J. Iron oxide based nanoparticles for multimodal imaging and magnetoresponsive therapy. *Chem. Rev.,* **2015**, *115*(19), 10637-10689.
http://dx.doi.org/10.1021/acs.chemrev.5b00112 PMID: 26250431

[58] Xu, H-L.; Mao, K-L.; Huang, Y-P.; Yang, J-J.; Xu, J.; Chen, P-P.; Fan, Z-L.; Zou, S.; Gao, Z-Z.; Yin, J-Y.; Xiao, J.; Lu, C-T.; Zhang,

B-L.; Zhao, Y-Z. Glioma-targeted superparamagnetic iron oxide nanoparticles as drug-carrying vehicles for theranostic effects. *Nanoscale,* **2016**, *8*(29), 14222-14236.
http://dx.doi.org/10.1039/C6NR02448C PMID: 27396404

[59] Dai, Y.; Yang, D.; Ma, P.; Kang, X.; Zhang, X.; Li, C.; Hou, Z.; Cheng, Z.; Lin, J. Doxorubicin conjugated NaYF(4):Yb($^{3+}$)/Tm($^{3+}$) nanoparticles for therapy and sensing of drug delivery by luminescence resonance energy transfer. *Biomaterials,* **2012**, *33*(33), 8704-8713.
http://dx.doi.org/10.1016/j.biomaterials.2012.08.029 PMID: 22938822